

LEARNING 3D PERCEPTION FROM OTHERS’ PREDICTIONS

Jinsu Yoo¹, Zhenyang Feng¹, Tai-Yu Pan¹, Yihong Sun², Cheng Perng Phoo², Xiangyu Chen²,
Mark Campbell², Kilian Q. Weinberger², Bharath Hariharan², and Wei-Lun Chao¹

¹The Ohio State University, ²Cornell University

ABSTRACT

Accurate 3D object detection in real-world environments requires a huge amount of annotated data with high quality. Acquiring such data is tedious and expensive, and often needs repeated effort when a new sensor is adopted or when the detector is deployed in a new environment. We investigate a new scenario to construct 3D object detectors: *learning from the predictions of a nearby unit that is equipped with an accurate detector*. For example, when a self-driving car enters a new area, it may learn from other traffic participants whose detectors have been optimized for that area. This setting is label-efficient, sensor-agnostic, and communication-efficient: nearby units only need to share the predictions with the ego agent (*e.g.*, car). Naively using the received predictions as ground-truths to train the detector for the ego car, however, leads to inferior performance. We systematically study the problem and identify viewpoint mismatches and mislocalization (due to synchronization and GPS errors) as the main causes, which unavoidably result in false positives, false negatives, and inaccurate pseudo labels. We propose a distance-based curriculum, first learning from closer units with similar viewpoints and subsequently improving the quality of other units’ predictions via self-training. We further demonstrate that an effective pseudo label refinement module can be trained with a handful of annotated data, largely reducing the data quantity necessary to train an object detector. We validate our approach on the recently released real-world collaborative driving dataset, using reference cars’ predictions as pseudo labels for the ego car. Extensive experiments including several scenarios (*e.g.*, different sensors, detectors, and domains) demonstrate the effectiveness of our approach toward label-efficient learning of 3D perception from other units’ predictions.¹

1 INTRODUCTION

Accurate detection of mobile objects (*e.g.*, vehicles, humans) in 3D is essential for an intelligent agent (*e.g.*, self-driving car, service robot) to operate safely and reliably (Lang et al., 2019; Shi et al., 2019; Wang et al., 2019; Shi et al., 2020). Constructing such a 3D object detector is never easy — it requires a huge amount of high-quality *labeled* data. Acquiring them is laborious and expensive, and is seldom a once-and-for-all effort. Whenever an agent enters a new environment and encounters new objects, its detector needs adaptation to remain accurate. Whenever a new sensor is adopted (*e.g.*, for energy or space efficiency), the different patterns in sensor data (*e.g.*, LiDAR point cloud style and density) necessitate the detector to be retrained. All these updates to the detector imply yet another round of tedious labeled data acquisition.

Could we bypass or, at least, reduce the repeated labeling effort? In this paper, we investigate the scenario in which there are other nearby agents equipped with accurate 3D object detectors (but not necessarily with the same sensor configuration). This scenario is realistic and promising. For example, self-driving taxis (*e.g.*, Waymo, Baidu) or local facilities (*e.g.*, surveillance systems, roadside units) are likely to be equipped with optimized detectors for their specific geo-fenced areas. While it may be infeasible for these local “experts” to directly share their raw sensor data or detectors (*e.g.*, due to data size and format; commercial and intellectual properties; implementation incompatibility), the *predictions* (*e.g.*, detected 3D bounding boxes) are more lightweight and standardized. Several

¹Project website: <https://jinsuyoo.info/rnb-pop>

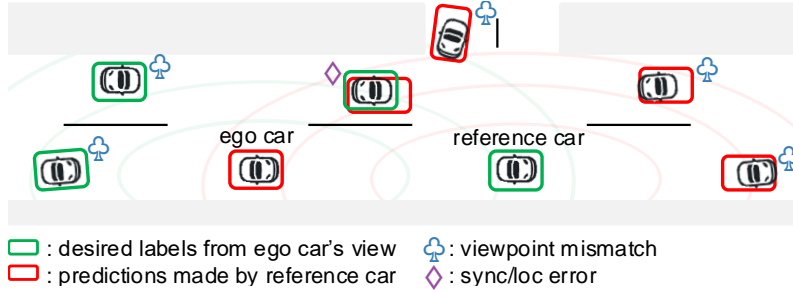


Figure 1: **Research problem of learning from others' predictions.** We study the scenario where an agent (*e.g.*, ego car) leverages the predictions made by another agent (*e.g.*, a high-end reference car) as supervision to train its own 3D object detector. We observe two challenges: (1) viewpoint mismatch between two cars and (2) mislocalization due to synchronization/GPS errors.

recent works also show that sharing predictions would benefit each participating agent's perception accuracy (Xu et al., 2023; 2022b; Yu et al., 2022; Chen et al., 2019; Xu et al., 2022a; Wang et al., 2020a; Lu et al., 2024; Hong et al., 2024; Hu et al., 2024), further incentivizing such a collaborative scenario. Last but not least, sharing predictions implies that there is no need for all the agents to use the same sensors. An agent adopting a new sensor or entering an unfamiliar environment thus could borrow the predictions made by other agents, potentially equipped with higher-end sensors, as labels to train its detector. (Please see Sec. 3.1 for a feasibility and practicality discussion of our setting.)

In this paper, we thus investigate a new scenario to construct a 3D object detector: *learning from the predictions of a nearby agent equipped with an accurate detector*. We use the real-world collaborative driving dataset (Xu et al., 2023) as the testbed. For each 3D road scene, this dataset records two LiDAR point clouds from two nearby cars distancing between 0 ~ 100 meters and offers object labels separately for each point cloud. We use one of the cars as the reference agent, equipped with an accurate 3D detector, to provide predicted labels from which the other (ego) car can learn.

At first glance, this research problem may appear trivially as a standard supervised learning problem — using another agent's predictions as labels to train the detector for the ego car. However, our preliminary attempt showed that this straightforward approach results in poor performance. We identify two major challenges (Fig. 1). First, in real-world applications, inaccuracies such as GPS errors and synchronization delays between agents are common. For example, a minor delay of just 0.1 seconds can cause a discrepancy of several meters in localization for a vehicle traveling at 60 mph. Second, the viewpoints of the two agents can vary significantly. An object visible to one agent might be obscured or out of range for the other due to occlusion or distance, leading to false positives and negatives in the predictions. Training with such *mislocalized* and *viewpoint-mismatched* labels inevitably results in suboptimal performance for the new 3D detector of the ego car.

To address these challenges, we propose a learning pipeline termed as *Refining & Discovering Boxes for 3D Perception from Others' Predictions (R&B-POP)*. For mislocalization, we train a box refinement module to rank the noisy candidates and correct their locations. Notably, this module requires very few human labels (1% or less), or even no human labels if simulation data are available. We also develop a coarse-to-fine approach to search for high-quality candidates around the predicted object locations efficiently, tackling large localization errors. For viewpoint mismatch that results in false negatives in the ego car's perspective, we present an effective self-training strategy empowered by a novel distance-based curriculum, enabling the detector to first learn from a subset of high-quality labels and in turn fill in the missing labels for the model to continually learn from. With these approaches, we significantly improve the quality of pseudo labels and, consequently, produce a much more accurate 3D detector for the ego car, with very limited human labeling — the Average Precision (AP) at IoU 0.5 increases from 22% to 56.5% using only 40 labeled frames!

In summary, we introduce a novel research problem that learns 3D perception for a new agent with reference agent's predictions. We identify the main challenges about the label quality and propose corresponding solutions. With extensive experiments, we demonstrate the applicability of the new learning scenario as well as the improvements achieved by our designs.

2 RELATED WORK

3D object detection serves an important role in real-world applications such as autonomous driving. The detector takes 3D signals (*e.g.*, LiDAR points) as input, and predicts the existence and the location of objects of interest. Notable development has been made thanks to the recently curated large datasets (Geiger et al., 2012; Caesar et al., 2020; Sun et al., 2020; Yu et al., 2022; Xu et al., 2023). The existing approaches can be categorized as voxel-based (or pillar-based) methods (Zhou & Tuzel, 2018; Yan et al., 2018; Lang et al., 2019), which subdivide irregular 3D point space into regular space, and point-based methods (Zhao et al., 2021; Yang et al., 2018), which directly extract discriminative point-wise features from the given point clouds. Regardless of approaches, these methods require manually annotated data of high-quality to achieve satisfactory performance. In this study, we aim to bypass such a labeling cost and demonstrate our new label-efficient learning method with representative 3D detectors (Lang et al., 2019; Yan et al., 2018).

Label-efficient learning. Self-supervised learning is a promising way to bypass extensive label annotation (Chen & He, 2021; He et al., 2020; Chen et al., 2020; Hjelm et al., 2018). Pre-trained with abundant, easily collectible unlabeled data, the detector backbone is shown to largely reduce the labeled data for fine-tuning (Pan et al., 2024; Yin et al., 2022; Xie et al., 2020b). Label-free 3D object detection from point clouds has gained attention due to its effective data utilization (You et al., 2022a;b; Luo et al., 2023; Najibi et al., 2022; Zhang et al., 2023; Choy et al., 2019; Baur et al., 2024; Seidenschwarz et al., 2024; Yang et al., 2021) and generalization beyond specific class information during training (Najibi et al., 2023). Orthogonally, we study a new scenario to learn the detector in a label-efficient way by considering *beyond a single source of information*. Specifically, the predictions from well-trained detectors of reference units near the ego car are leveraged as (pseudo) labels.

Domain adaptation. Our setting is related to domain adaptation (DA), as we aim to improve an object detector in a new environment (*e.g.*, a new location or data pattern). Existing studies (Wang et al., 2020b; Chen et al., 2024; Yang et al., 2021; 2022) mostly focus on the generic, single-agent unsupervised DA setting, while a few leverage application-specific cues, *e.g.*, repetitions (You et al., 2022c), to facilitate adaptation. Our setting belongs to the second branch, in which we explore a multi-agent scenario. Our goal is not to compete with the generic setting. Instead, generic DA techniques, *e.g.*, advanced self-training (Peng et al., 2023; Wang et al., 2023; Hegde et al., 2023; Tsai et al., 2023), can be compatible with our setting to further boost the performance.

Curriculum learning. Many studies have shown that properly ordering the data to progressively add harder samples during training leads to superior performance. The so-called “curriculum learning” (Bengio et al., 2009) has also been explored in object detection (Li et al., 2017; Sangineto et al., 2018). For LiDAR-based 3D detection, researchers have applied the concept for better data augmentation during training (Yang et al., 2021; Zhu et al., 2023). We investigate the task-specific characteristics from the data and discover a meaningful correlation between the label quality and the ego-car-reference-car distance. We then apply this observation to design an effective training curriculum.

Collaborative perception. To mitigate limited detection range and occlusion, self-driving researchers have recently focused on integrating nearby detectors’ information (Chen et al., 2019; Xu et al., 2022b;a; 2023; Yu et al., 2022; Wang et al., 2020a; Lu et al., 2024; Hong et al., 2024; Hu et al., 2024). During inference, more than one detector communicates with each other and shares their information (*e.g.*, input signal, feature, or predicted boxes) to detect objects better. While also leveraging other cars’ information, our research focus is different — we investigate a new label-efficient learning scenario, using other (expert) cars’ predictions as supervision to build the ego car’s detector offline.

3 LEARNING 3D PERCEPTION FROM OTHERS’ PREDICTIONS

We study a novel research problem in autonomous driving: training a 3D detector using bounding boxes supplied by a nearby agent. This scenario, while unexplored, can reduce or even eliminate labeling efforts. We identify the key challenges and propose the learning pipeline to address them.

3.1 PROBLEM DEFINITION AND FEASIBILITY

Problem setup. Without loss of generality, we assume that around the ego car (*i.e.*, E), there is a reference car (*i.e.*, R) equipped with an accurate 3D object detector f_R . E and R are both equipped

Table 1: **Label quality** in recall and precision at IoU 0.5 with E 's GT. Our methods improve the label quality significantly.

pseudo label	R 's GT		R 's pred	
	rec. / prec.	rec. / prec.	rec. / prec.	rec. / prec.
① initial boxes	54.8 / 43.2	56.1 / 48.0		
② + basic filtering	54.1 / 65.6	55.3 / 71.4		
③ + our refinement	66.2 / 85.4	65.2 / 79.0		
④ + our self-train	72.5 / 90.0	74.4 / 87.7		
⑤ sharing detector	-	78.8 / 86.8		

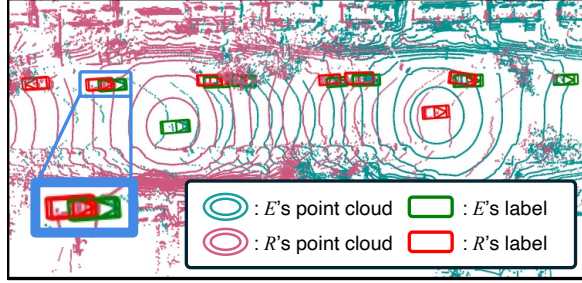


Figure 2: **Point and box discrepancies** between ego and reference cars on the real dataset (Xu et al., 2023).

with 3D sensors (e.g., LiDAR) and collect their point clouds (i.e., X_E and X_R) in the same road scene. Notice that X_E and X_R can have different patterns due to variations in hardware. R , the car that E learns from, share 3D bounding boxes of foreground objects in the global coordinate from its detector, i.e., $Y_R = f_R(X_R)$. Our goal is to train a 3D detector f_E that works with X_E , by using Y_R .

Feasibility and practicality. Before proceeding, we consider two critical questions, “Why can nearby agents obtain accurate detectors?” and “Why can they not directly share their detectors?” Besides the examples mentioned in Sec. 1 (e.g., self-driving taxis), we emphasize that these nearby agents need not be “omniscient.” Instead, they only need to be experts in geo-fenced areas where the ego agent passes by and can even be static, making training their detectors easier and much more label-efficient, e.g., using the repetition or background cues (You et al., 2022b;a; Dao et al., 2024).

Regarding “why these agents cannot just share their detectors,” we note that while open-sourcing is common in the research community, there are many considerations and constraints when it comes to practical scenarios. First, the ego and the reference agents do not need to have the same sensors. Indeed, they may not even perceive the environment from the same views, e.g., the reference agent can be a roadside unit placed six meters high and facing down (Yang et al., 2023; Dao et al., 2024). This discrepancy makes the direct deployment of the reference agent’s model to the ego agent suboptimal. Second, the two agents may be equipped with different computational platforms, e.g., the reference one is equipped with GPUs while the ego one with FPGA boards and hardware acceleration code (Hao et al., 2019; Hao & Chen, 2021), making direct deployment more challenging. Last but not least, reference agents’ detectors may be specifically designed and trained, e.g., using private data. Sharing them thus raises intelligent property or privacy concerns. Putting things together, we argue that our setting is realistic and has significant practical implications.

3.2 CHALLENGE

First attempt. We use the recently released real-world collaborative driving dataset (Xu et al., 2023) as the testbed. For each 3D road scene (with a time tag), the dataset provides LiDAR point clouds and ground-truth 3D bounding boxes from each agent’s perspective. (We keep the data and experimental details in Sec. 4.) We begin by employing Y_R (i.e., R ’s predictions) directly as labels for E to train f_E , after transforming Y_R into E ’s coordinate system. To establish an upper bound, we also train a detector using E ’s ground-truth labels. The result shows that the detector performance by naively using Y_R is way much worse than the upper bound (AP at IoU 0.5: ① 22.0 vs. ♣ 58.4 in Table 2).

At first glance, such a gap, with no doubt, must come from reference car R ’s prediction errors. To eliminate the effect, we use R ’s ground-truths as labels (i.e., R ’s GT) to train another detector for the ego car E . To our surprise, using R ’s GT can hardly improve the detector’s performance, suggesting the existence of other, more fundamental factors in the real-world environment.

Key challenges. To search for the root cause of the poor detector performance, we visualize the point clouds and ground-truth bounding boxes of the two cars in Fig. 2. We identify two major sources of errors: viewpoint mismatch and mislocalization. Viewpoint mismatch occurs when objects are obscured from one sensor’s view due to occlusion or field of view limitations, while mislocalization results from GPS inaccuracies and synchronization delays. For instance, a communication delay of 0.1 seconds in a car traveling at 60 mph can result in a localization discrepancy of 2.7 meters. These errors can significantly degrade the quality of the learned detector f_E for the ego car E — the training

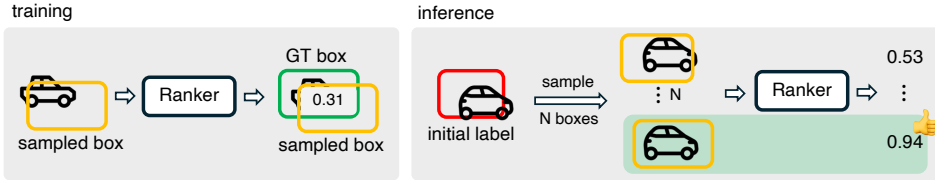


Figure 4: **Box ranker for refining localization error.** With a few annotated frames (or boxes), we train a ranker that can estimate the quality of a given box. During inference for pseudo labels, we sample multiple candidates near the initial noisy box and choose the one with the best IoU.

labels are simply *noisy*. To further dive into these challenges, we measure the precision and recall of Y_R vs. the ego car E 's ground-truth labels to assess label quality, as shown in Table 1. Even after applying basic filtering commonly used in autonomous driving (e.g., removing distant boxes or those with few points that are beyond E 's field of view), the label quality remains unsatisfactory (Table 1 ②). In the following sections, we introduce our pipeline R&B-POP to tackle these challenges.

3.3 LABEL-EFFICIENT BOX REFINEMENT

Preliminaries. We conduct a detailed analysis of the localization discrepancies in each coordinate (x forward, y leftward, z upward) between R 's and E 's overlapping ground-truth boxes, as illustrated in Fig. 3. Notice that a mere 0.5-meter discrepancy in the x and y coordinates can drastically reduce the IoU from 100% to 30%. Training with such inaccurate pseudo labels inevitably leads to suboptimal performance in E 's 3D detector. A refinement module for the labels is thus necessary!

Baseline approach with heuristics. To begin with, we adopt the algorithm proposed in Luo et al. (2023), which refines boxes using heuristics. Specifically, multiple boxes are sampled around the initial noisy boxes, and the optimal boxes are selected based on the best alignment of edges and sizes between the boxes and point clouds. However, this method requires certain conditions to achieve satisfactory performance, such as multiple trajectories at the same location, potentially limiting the applicability. As in Table 2, adapting it to our problem brings marginal gains, especially for the high IoU of 0.7 (AP ① 4.2 vs. ③ 10.3).

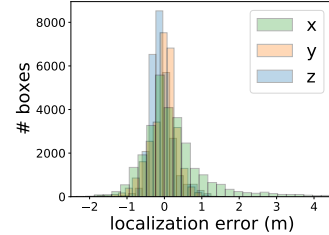


Figure 3: **Mislocalization** between E 's and R 's GT.

Label-efficient box ranker. To address this limitation, we propose to train a *box ranker* that evaluates the localization quality of given bounding boxes. Instead of predicting a 3D box from scratch (i.e., a typical detection problem), learning to select and adjust among noisy candidates is a much easier task. We thus expect learning such a ranker needs much fewer labeled data! To investigate this idea, we sample a handful of E 's point clouds with ground-truths to train the ranker. We randomly sample multiple boxes around each annotated object box and crop point clouds outlined by those sampled boxes (with expansion). The training objective is dual: to regress the IoU between a sampled box and the annotated box, serving as the indicator of localization quality, and to estimate the offset to the annotated box, further refining its location. During inference, we use Y_R as initial boxes and sample N boxes around each. The top-ranked boxes are selected among all candidates to construct Y'_R as pseudo labels for training the 3D detector f_E for E (see Fig. 4). We adopt a neural network similar to PointNet (Qi et al., 2017) for the ranker for its simplicity. Please see the supplementary for details.

Coarse-to-fine (C2F) refinement. As previously discussed, minor time delays can result in large discrepancies of several meters. To address this and expand the search region, thereby increasing the number of high-quality bounding box candidates for our ranker, we employ a two-stage approach during *inference*, as illustrated in Fig. 5. In the first stage, we generate $\frac{N}{2}$ candidate boxes for each initial box by sampling uniform translations from a wider range using a uniform distribution, while keeping the scale and pose of the boxes fixed. In the second stage, we select the top- K boxes from the first stage to serve as new initials and sample another $\frac{N}{2}$ total new boxes

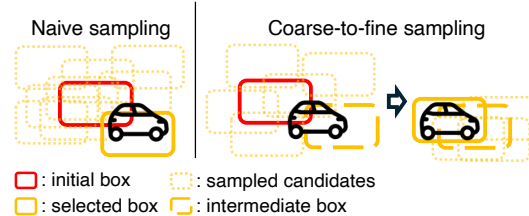


Figure 5: **Sampling methods for box refinement.** Proposed C2F is more effective in large mislocalization.



Figure 6: **Overall pipeline of R&B-POP.** The ego car first receives reference’s predictions which contain inherent noises (Sec. 3). It refines their localization with proposed box ranker (Sec. 3.3). Then, it creates high-quality pseudo labels by distance-based curriculum for self-training (Sec. 3.4).

around them, this time considering all degrees of freedom (*i.e.*, translation, scale, and pose) but from a narrower range using normal distributions. This coarse-to-fine (C2F) strategy effectively bridges the large localization gap and enhances the refinement quality of Y'_R . With the box ranker and C2F, we raise the label quality from a recall of 55.3 to 65.2 and a precision of 71.4 to 79.0 upon basic filtering, as shown in Table 1 ② vs.③, using only 40 labeled frames. Consequently, the performance of f_E also shows a significant gain from 22.0% to 38.0% in AP at IoU 0.5, as reported in Table 2 ① vs.④.

Ranker-based filtering. The trained ranker not only refines the given boxes but also estimates their IoU with ground-truth boxes. Applying a threshold on predicted IoU effectively removes false positives, thus improving detection performance as shown in Table 4b.

3.4 DISTANCE-BASED CURRICULUM

Viewpoint mismatch introduces false positives (*i.e.*, objects should not be visible from E ’s perspective) and negatives (*i.e.*, objects should be visible to E but are not provided by R) in Y_R . While false positives can be removed by filtering (*e.g.*, basic and ranker-based filtering), false negatives are much harder to be recovered. It becomes necessary to discover new boxes from E ’s perspective.

Box discovery from the ego car E ’s view. Inspired by the previous work (You et al., 2022b), self-training (Lee et al., 2013; Xie et al., 2020a) is a popular technique to propagate labels to unlabeled data. This method typically employs high-quality labels to train the base detector and subsequently uses its predictions to generate new pseudo labels for further fine-tuning cycles. However, as discussed in previous sections, our initial (pseudo) labels are inherently noisy, which can hinder the efficacy of self-training. This leads to a pivotal question: *How to ensure the quality of pseudo labels for effective self-training?*

Key observation about distance. We find out that there exists a unique property in our learning scenario — the extent of viewpoint mismatch is correlated with the distance between E and R . Specifically, discrepancies are typically reduced when the two are closer and increased when they are distant (Fig. 7). This intuition leads us to use the distance of two cars as an indicator of the quality of pseudo labels provided by R . Building on this observation, we develop two distance-based methods in the following.

Distance-based curriculum for self-training. We create a high-quality subset of pseudo labels by applying a simple distance threshold T_{E-R} to all frames, meaning that we trust pseudo labels from R when two cars are close enough. In the first round of self-training, the 3D detector f_E is exclusively trained on this high-quality subset. In later rounds, we fine-tune on *all frames* with pseudo labels predicted by F_E . This approach propagates labels learned from confident frames to unconfident ones.

Distance-based filtering. Self-training needs a filtering mechanism to select high-quality predictions by the current detector, which are then treated as true labels to supervise the next round of detector

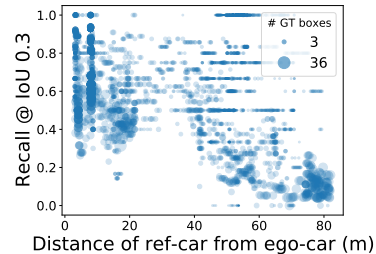


Figure 7: **Quality of pseudo labels from R ’s predictions** drops when two cars are farther apart.

training. Normally, this is done by setting a fixed threshold T_c in prediction confidence². Here, we employ a distance-based threshold, inspired by our self-training procedure. Specifically, since we trust frames with smaller ego-car-to-reference-car distances and train the detector with them in the first round, the detector will inherently be overly confident in these frames. As such, a higher threshold shall be assigned when selecting pseudo labels from them. We implement this idea by increasing the confidence threshold with a negative linear function of the distance (*i.e.*, $T_c + \lambda/distance(E, R)$).

Put together, these two distance-based approaches not only uncover boxes that should be visible to E but also preserve the quality of pseudo labels for self-training. As shown in Table 1 ④, self-training with distance-based curriculum further improves label quality from 79.0% to 87.7% in precision and 65.2% to 74.4% in recall, resulting in an enhancement of f_E 's performance from AP of 38.0% to 56.5%, as detailed in Table 2 ④ vs. ⑩. As a reference, we show the predicted label quality on X_E using f_R in Table 1 ⑤, simulating the ideal case where the object detector can be shared. Our R&B-POP achieves similar label quality, demonstrating the applicability of our setting for learning high-quality detectors from others' predictions.

3.5 OVERALL PIPELINE

Putting everything together, our overall *offline* pipeline involves the following steps (Fig. 6).

Step 0. Ranker training with few annotated labels (Sec. 3.3).

Step 1. First-round self-training: Preparing pseudo labels after receiving R 's predictions (applying basic filtering), further improving labels with ranker + C2F and ranker-thresholding (Sec. 3.3), and then training the detector f_E with closer frames (Sec. 3.4).

Step 2. Second-round self-training: Preparing pseudo labels after receiving f_E 's prediction (applying distance-filtering in Sec. 3.4), further improving labels with ranker + C2F and ranker-thresholding (Sec. 3.3), and then training the detector f_E with all frames.

4 EXPERIMENTS

4.1 EXPERIMENTAL SETUPS

Datasets. To validate the effectiveness of our method, we conduct experiments primarily on the V2V4Real dataset (Xu et al., 2023), which consists of 40 clips with a total of 18k frames by driving two cars, Tesla and Honda, together within 100m. LiDAR points are acquired with a Velodyne VLP-32 LiDAR sensor. The dataset provides annotations for different types of vehicles, such as cars and trucks. (Please see additional results on the OPV2V dataset (Xu et al., 2022c) in the supplementary.)

To align with our research purpose, we re-split the original data into three portions: " R pretraining", " R prediction/ E training", and " E validation/test" (Fig. 8). Specifically, we split them into two subsets containing 20 clips and use the first subset to pre-train R 's detector f_R . Then we inference on the second subset to provide pseudo labels Y_R for training E 's detector f_E together with E 's point clouds. We validate and test the E 's performance on the first subset by splitting it into 20% and 80%. Our re-split gives 4,488 frames for R pretraining, $4,463 \times 2$ frames for E training, and 870 and 3,618 frames for E validation/test respectively. The performance in the paper is reported on E 's test set.

Evaluation. We follow Xu et al. (2023) to merge different types of vehicles (*e.g.*, cars, trucks) into a single category³. We report the average precision (AP) of detectors in the bird's-eye view with

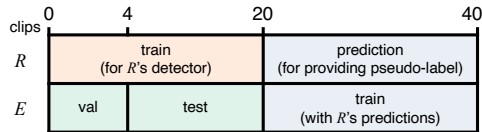


Figure 8: **Dataset split.** We re-split V2V4Real (Xu et al., 2023) for our setting.

²We note that the detector's confidence is not the same as the IoU predicted by the ranker in Sec. 3.3.

³We note that V2V4Real (Xu et al., 2023) does not label objects beyond vehicles and the data distributions across different types of vehicles are largely imbalanced. Thus, it is infeasible to study multi-class vehicle detection. That said, extending our approach to a multi-class setup would be straightforward if a suitable dataset is available. The key is to make the ranker category aware. Please refer to our experiments on extending the ranker to a multi-class setting in the supplementary.

Table 2: **Main results: validation of the proposed learning scenario and methods.** The results indicate a new research problem of *learning with others’ predictions* has inherent challenges. With proposed R&B-POP, we significantly close the gap to the upper bound that directly uses ego car’s ground-truth labels (♠ 56.5 vs. ♣ 58.4). The performance is reported on PointPillars (Lang et al., 2019) with 32-beam LiDAR. : uses GT labels. : our proposed methods.

	pseudo label	box refinement	self-training	AP @ IoU 0.5				AP @ IoU 0.7			
				0-30m	30-50m	50-80m	0-80m	0-30m	30-50m	50-80m	0-80m
①	<i>R</i> ’s pred	-	-	34.7	13.5	8.6	22.0	7.6	2.2	1.5	4.2
②	<i>R</i> ’s GT	-	-	29.7	14.1	7.3	19.6	5.9	2.2	1.8	3.7
③	<i>R</i> ’s pred	heuristic (Luo et al., 2023)	-	53.2	22.0	16.9	37.8	16.5	4.5	3.9	10.3
④	<i>R</i> ’s pred	ranker	-	50.3	24.7	18.2	38.0	33.6	12.9	8.9	22.9
⑤	<i>R</i> ’s pred	-	naïve (You et al., 2022b)	45.9	18.7	16.5	32.4	13.8	4.6	5.9	9.2
⑥	<i>R</i> ’s pred	heuristic (Luo et al., 2023)	naïve (You et al., 2022b)	50.4	19.6	15.4	35.4	13.8	4.2	3.6	8.9
⑦	<i>R</i> ’s pred	ranker	naïve (You et al., 2022b)	60.6	29.7	19.2	45.0	40.8	16.7	9.5	28.0
⑧	<i>R</i> ’s pred	-	distance-based curriculum	57.3	29.6	21.0	42.5	21.0	5.9	3.9	12.7
⑨	<i>R</i> ’s pred	heuristic (Luo et al., 2023)	distance-based curriculum	60.5	25.5	17.0	43.2	18.3	4.4	3.0	11.0
⑩	<i>R</i> ’s pred	ranker	distance-based curriculum	73.3	43.3	23.3	56.5	47.1	21.1	10.0	32.6
♣	<i>E</i> ’s GT	-	-	75.2	45.9	28.8	58.4	51.7	25.4	14.8	36.3

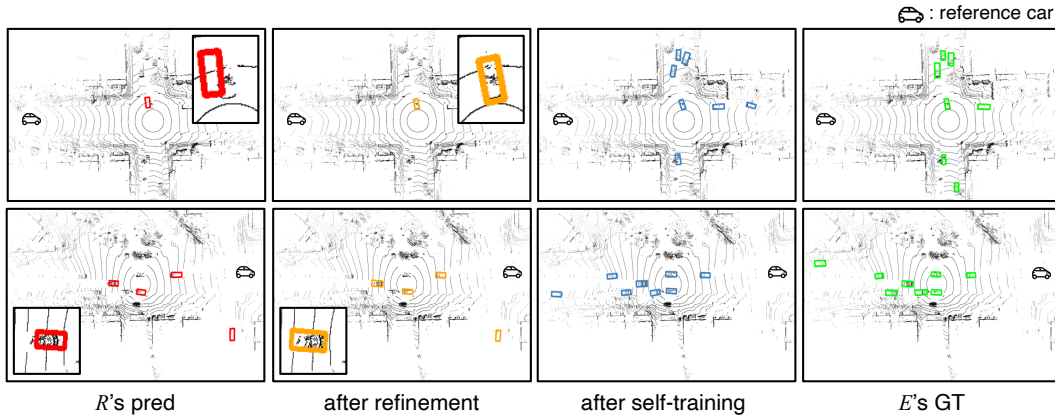


Figure 9: **Qualitative results.** The quality of pseudo labels is gradually improved with the proposed R&B-POP. Our ranker successfully fixes mislocalization errors, and distance-based curriculum further discovers new objects from *E*’s view.

IoU thresholds of 0.5 and 0.7. Specifically, we set the region of interest to $[-80, 80]$ m for the heading direction and $[-40, 40]$ m for the direction perpendicular to the moving direction. We also report the AP on different depth ranges $[0-30, 30-50, 50-80, 0-80]$ m following Luo et al. (2023).

Implementation. We conduct experiments with PointPillars (Lang et al., 2019) as a default **detector**. We train it with 60 epochs and a batch size of 64 on 8 NVIDIA Tesla P100 GPUs. We use Adam optimizer and an initial learning rate of $2e-3$ dropped to $2e-5$ by cosine annealing decaying strategy (Loshchilov & Hutter, 2017). For training the **box ranker**, a PointNet (Qi et al., 2017) specified in the supplementary, we use 40 annotated frames ($< 1\%$ of training data) to generate 11k samples. In the *offline* ranker inference, we sample $N = 512$ boxes around each prediction provided by the reference car. We first sample 256 boxes in the coarse stage, select top-3 boxes, and then sample the remaining 256 boxes near the selected boxes in the fine stage. For curriculum learning, we set T_{E-R} to 40m. Also, we set the ranker threshold to 0.5, and λ for the distance-based threshold to 1 with a fixed confidence threshold T_c of 0.2. Please refer to the supplementary material for more details.

4.2 EXPERIMENTAL RESULTS

We first demonstrate our scenario, *learning with others’ predictions*, with a basic setup: *R* and *E* both have 32-beam sensors with PointPillars (Lang et al., 2019), but only *R*’s detector was pre-trained. Table 2 compares different methods for pseudo labels, including baselines such as standard self-training (You et al., 2022b) and heuristic-based label refinement (Luo et al., 2023). For fair comparisons, we note that we only utilize annotated boxes from 40 frames to train our ranker, not to train the

Table 3: **Ablations on box ranker.** (a) The training of the ranker requires very few human labels. Using simulation data further eliminates the need yet performs on par. (b) The proposed inference strategies effectively generate high-quality pseudo labels, resulting in better performance.

training data	# annot. frames	AP @ IoU		sampling			AP @ IoU	
		0.5	0.7	offset	naive	C2F	0.5	0.7
E 's GT	20	54.8	30.0	①	✓		50.2	28.5
	40	56.5	32.6	②	✓	✓	56.5	30.7
	80	55.5	32.8	③	✓		56.5	32.6
Simulation (Xu et al., 2022c)	21k	52.2	28.4	④		✓	54.4	31.0

(a) Analysis on training labels.

(b) Analysis on inference strategies.

Table 4: **Ablations on curriculum self-training.** The results show that each individual component in our proposed method contributes to the optimal performance. (a) Our curriculum selectively leverages useful frames during each stage of training. (b) Our label thresholding effectively discards noisy labels for training, resulting in improved performance.

	pseudo label		AP @ IoU		AP @ IoU			
	stage 1	stage 2	0.5	0.7	ranker threshold	distance-based threshold	0.5	0.7
①	0-90m	0-90m	45.0	28.0				
②	0-40m	0-40m	50.3	24.7			54.9	30.3
③	0-40m	40-90m	51.1	26.0		✓	52.2	28.3
④	40-90m	40-90m	33.5	20.0			56.5	32.6
⑤	0-40m	0-90m	56.5	32.6	✓	✓		

(a) Analysis on different curriculums.

(b) Analysis on box filtering.

detector. For the heuristic-based refinement (Luo et al., 2023), as our dataset has no repeated traversal to estimate movable objects, we use RANSAC (Fischler & Bolles, 1981) instead.

Firstly, our ranker brings a notable gain over heuristics-based refinement (③ 10.3 vs. ④ 22.9, ⑥ 8.9 vs. ⑦ 28.0, and ⑨ 11.0 vs. ⑩ 32.6 on AP at IoU 0.7), demonstrating its effectiveness to address mislocalization. Secondly, our distance-based curriculum consistently improves the performance over the standard self-training (⑤-⑦ 32.4/35.4/45.0 vs. ⑧-⑩ 42.5/43.2/56.5), demonstrating the necessity of using higher-quality samples for self-training. Finally, by comparing with detectors trained with E 's ground-truth, our method achieves on par with the upper bound (⑩ 56.5/32.6 vs. ♣ 58.4/36.3).

Fig. 9 visualizes the improvement of pseudo labels with our method. The ranker successfully refines mislocalized pseudo labels provided by R . Moreover, our distance-based curriculum discovers new bounding boxes that E couldn't receive from R 's perception, without introducing many false positives.

4.2.1 ABLATION STUDY

Analysis on ranker training. We first check the performance of the ranker trained with different number of annotated frames (*i.e.*, 20, 40, and 80) in Table 3a. Notably, we observe a performance boost when the ranker is trained with 40 frames compared to 20 frames, and the performance gain diminishes with more than 40 frames. This demonstrates that the ranker already perform well with very few labeled data (*i.e.*, 1% of total). Moreover, we train our ranker with 21k samples generated by CARLA simulator (Xu et al., 2022c) and achieves on par performance, exploring to remove the need of human labels.

Analysis on ranker inference. We investigate the impact of inference strategies for the refinement on the final detection performance in Table 3b. The results indicate that sampling boxes (① 28.5 vs. ② 30.7) and coarse-to-fine refinement (② 30.7 vs. ③ 32.6) contribute to superior performance, especially for the fine-grained quality of IoU 0.7. We also observe the benefit of using predicted offsets to further refine box locations (④ 31.0 vs. ③ 32.6). This demonstrates the effectiveness of our sophisticated box refinement strategies.

Analysis on curriculum for self-training. In our method, we split the training data into two subsets with the threshold T_{E-R} of 40m. We train the detector on different combinations of subsets and check

Table 5: **Application to different scenarios.** We study cases where E and R have different LiDAR patterns or detector architectures. We further equip E with a pre-trained detector aiming to adapt to R 's driving scenes. The results indicate the flexibility of the new research problem of *learning from others' predictions*. [†]We use simulation data collected by Xu et al. (2022c).

				AP @ IoU							
		E 's detector	R 's detector	0.5	0.7			AP @ IoU			
# beams	AP @ IoU										
R	E	0.5	0.7			label from		0.5	0.7		
8	32	54.8	31.6	SECOND	PointPillars	56.2	37.2	pre-trained (PT)	CALRA [†]	51.7	32.5
16	32	56.0	31.5	PointPillars	PointPillars	56.7	37.3	fine-tuned	PT	58.0	35.0
32	32	56.5	32.6		E 's GT	63.8	43.9		PT + R 's pred	60.8	37.7

(a) Different sensors.

(b) Different detectors.

(c) Domain adaptation.

its performance (Table 4a). We observe that using initial low-quality frames to train the model gives significantly lower performance (④ 33.5 vs. ⑤ 56.5). Also, we see that the performance escalates as we utilize more high-quality frames during the next self-training stage (② 50.3, ③ 51.1 vs. ⑤ 56.5), verifying the effectiveness of our curriculum choice.

Analysis on box filtering for self-training. To prevent the model from introducing false positive boxes during the self-training, we design a distance-based confidence threshold and ranker-based filtering. As shown in Table 4b, the detector improves with our strategies. This indicates a good balance between recall and precision provided by our method, resulting in better detection performance.

4.2.2 APPLICATIONS TO DIFFERENT SCENARIOS

R&B-POP can also be used when E and R have different detectors and hardware sensors, and are across different domains. This section evidences the flexibility of our method.

Different sensors. To show that our pipeline can be trained on facilities with different sensors, we conduct experiments with synthesized 16- and 8-beam LiDAR point clouds with the beam-dropping algorithm (Wei et al., 2022). Specifically, we assume R has either 8-, 16-, and 32-beam, respectively, and the detector architecture is fixed to PointPillars (Lang et al., 2019). As shown in Table 5a, the detection performance does not drop when using less advanced sensors (*i.e.*, fewer beams). This indicates the flexibility of our algorithm in different sensor configurations.

Different detectors. We conduct experiments to demonstrate the effectiveness of our pipeline on different detectors, *e.g.*, PointPillars (Lang et al., 2019) and SECOND (Yan et al., 2018), by using various combinations in Table 5b. The results show that the detector performance of E does not rely on R 's detector, which implies E tends to learn agnostically to R 's setups. Together with the experiments for different sensors, this highlights the general flexibility of our method.

Different domains. We explore our algorithm's applicability to the domain adaptation scenario with a synthetic to real case. In doing so, we assume that E 's detector has been pre-trained on simulation data (Xu et al., 2022c). As shown in Table 5c, the performance of E 's pre-trained detector improves with adaptation to real domains (via self-training). Notably, we compare adaptation with and without using R 's predictions and observe that leveraging the predicted boxes from R is beneficial.

4.2.3 ADDITIONAL EMPIRICAL STUDIES

We leave additional results in the supplementary, including the ideal scenario where the object detector can be shared, analysis on ranker and self-training, and extension to another dataset.

5 CONCLUSION AND DISCUSSION

In this work, we have introduced *learning with others' predictions*, a new way to train a 3D detector with the predictions of reference units. We have systematically identified the inevitable task-specific problems: false positive, false negative, and noisy boxes due to either viewpoint mismatch or synchronization/GPS errors. Next, we have proposed to improve the quality of pseudo labels by two

solutions: A box ranker and distance-based curriculum self-training. We have demonstrated a wide applicability of our learning scenario with different detectors, sensors, and domains.

Limitations and future work. The ego car’s detector can benefit from other reference units, such as roadside units in smart cities. In our future work, we plan to investigate more diverse scenarios. Moreover, the ego car and the reference car using different modalities would be a direction to explore further. We believe that our findings and approach have set the foundation for it. At a high level, our approach is sensor and modality-agnostic. Regardless of the type of sensors and detectors (camera-based or LiDAR-based) used, if we aim at 3D perception, they will produce 3D bounding boxes as pseudo labels. Our method does not necessitate a specific model for providing the pseudo labels and can be easily adapted to various sensor types. We leave this extension to future work.

ACKNOWLEDGMENT

This research is supported in part by grants from the National Science Foundation (IIS-2107077, IIS-2107161, III-1526012, and IIS-1149882) and NVIDIA research. We are thankful for the generous support of the computational resources by the Ohio Supercomputer Center.

ETHICS STATEMENT

We investigate a collaborative scenario in which higher-end detectors’ predictions would ease other perception agents’ labeling efforts in training their perception systems. In this paper, we focus on how to unleash the benefit of such a collaborative scenario, assuming that all the participating agents are benign. In practice, however, malicious agents may appear and degrade the overall pipeline. How to deal with malicious agents and data has been one of the main topics in AI with many robust solutions being proposed. We expect that these existing solutions can be incorporated into our work to mitigate potentially malicious situations.

REPRODUCIBILITY STATEMENT

We plan to make our implementation publicly available to promote reproducibility. Moreover, the implementation details, including all hyperparameters, model architectures, datasets, computational resources, and evaluation metrics, are provided in both the main paper (Sec. 4.1) and the supplementary material (Sec. S1).

REFERENCES

- Stefan Baur, Frank Moosmann, and Andreas Geiger. Liso: Lidar-only self-supervised 3d object detection. In *ECCV*, 2024.
- Yoshua Bengio, Jérôme Louradour, Ronan Collobert, and Jason Weston. Curriculum learning. In *ICML*, 2009.
- Holger Caesar, Varun Bankiti, Alex H Lang, Sourabh Vora, Venice Erin Liong, Qiang Xu, Anush Krishnan, Yu Pan, Giancarlo Baldan, and Oscar Beijbom. nuscenes: A multimodal dataset for autonomous driving. In *CVPR*, 2020.
- Qi Chen, Xu Ma, Sihai Tang, Jingda Guo, Qing Yang, and Song Fu. F-cooper: Feature based cooperative perception for autonomous vehicle edge computing system using 3d point clouds. In *ACM/IEEE Symposium on Edge Computing*, 2019.
- Ting Chen, Simon Kornblith, Mohammad Norouzi, and Geoffrey Hinton. A simple framework for contrastive learning of visual representations. In *ICML*, 2020.
- Xiangyu Chen, Zhenzhen Liu, Katie Z Luo, Siddhartha Datta, Adhitya Polavaram, Yan Wang, Yurong You, Boyi Li, Marco Pavone, Wei-Lun Chao, et al. Diffubox: Refining 3d object detection with point diffusion. In *NeurIPS*, 2024.
- Xinlei Chen and Kaiming He. Exploring simple siamese representation learning. In *CVPR*, 2021.

- Christopher Choy, JunYoung Gwak, and Silvio Savarese. 4d spatio-temporal convnets: Minkowski convolutional neural networks. In *CVPR*, 2019.
- Minh-Quan Dao, Holger Caesar, Julie Stephany Berrio, Mao Shan, Stewart Worrall, Vincent Frémont, and Ezio Malis. Label-efficient 3d object detection for road-side units. In *IV*, 2024.
- Martin A Fischler and Robert C Bolles. Random sample consensus: a paradigm for model fitting with applications to image analysis and automated cartography. *Communications of the ACM*, 1981.
- Andreas Geiger, Philip Lenz, and Raquel Urtasun. Are we ready for autonomous driving? the kitti vision benchmark suite. In *CVPR*, 2012.
- Cong Hao and Deming Chen. Software/hardware co-design for multi-modal multi-task learning in autonomous systems. In *AICAS*, 2021.
- Cong Hao, Atif Sarwari, Zhijie Jin, Husam Abu-Haimed, Daryl Sew, Yuhong Li, Xinheng Liu, Bryan Wu, Dongdong Fu, Junli Gu, et al. A hybrid gpu+ fpga system design for autonomous driving cars. In *SiPS*, 2019.
- Kaiming He, Haoqi Fan, Yuxin Wu, Saining Xie, and Ross Girshick. Momentum contrast for unsupervised visual representation learning. In *CVPR*, 2020.
- Deepti Hegde, Velat Kilic, Vishwanath Sindagi, A Brinton Cooper, Mark Foster, and Vishal M Patel. Source-free unsupervised domain adaptation for 3d object detection in adverse weather. In *ICRA*, 2023.
- R Devon Hjelm, Alex Fedorov, Samuel Lavoie-Marchildon, Karan Grewal, Phil Bachman, Adam Trischler, and Yoshua Bengio. Learning deep representations by mutual information estimation and maximization. *arXiv preprint arXiv:1808.06670*, 2018.
- Shixin Hong, Yu Liu, Zhi Li, Shaohui Li, and You He. Multi-agent collaborative perception via motion-aware robust communication network. In *CVPR*, 2024.
- Yue Hu, Juntong Peng, Sifei Liu, Junhao Ge, Si Liu, and Siheng Chen. Communication-efficient collaborative perception via information filling with codebook. In *CVPR*, 2024.
- Alex H Lang, Sourabh Vora, Holger Caesar, Lubing Zhou, Jiong Yang, and Oscar Beijbom. Pointpillars: Fast encoders for object detection from point clouds. In *CVPR*, 2019.
- Dong-Hyun Lee et al. Pseudo-label: The simple and efficient semi-supervised learning method for deep neural networks. In *ICML Workshop*, 2013.
- Siyang Li, Xiangxin Zhu, Qin Huang, Hao Xu, and C-C Jay Kuo. Multiple instance curriculum learning for weakly supervised object detection. *arXiv preprint arXiv:1711.09191*, 2017.
- Ilya Loshchilov and Frank Hutter. Decoupled weight decay regularization. *arXiv preprint arXiv:1711.05101*, 2017.
- Yifan Lu, Yue Hu, Yiqi Zhong, Dequan Wang, Siheng Chen, and Yanfeng Wang. An extensible framework for open heterogeneous collaborative perception. In *ICLR*, 2024.
- Katie Z Luo, Zhenzhen Liu, Xiangyu Chen, Yurong You, Sagie Benaïm, Cheng Perng Phoo, Mark Campbell, Wen Sun, Bharath Hariharan, and Kilian Q. Weinberger. Reward finetuning for faster and more accurate unsupervised object discovery. In *NeurIPS*, 2023.
- Mahyar Najibi, Jingwei Ji, Yin Zhou, Charles R Qi, Xinchun Yan, Scott Ettinger, and Dragomir Anguelov. Motion inspired unsupervised perception and prediction in autonomous driving. In *ECCV*, 2022.
- Mahyar Najibi, Jingwei Ji, Yin Zhou, Charles R Qi, Xinchun Yan, Scott Ettinger, and Dragomir Anguelov. Unsupervised 3d perception with 2d vision-language distillation for autonomous driving. In *ICCV*, 2023.

- Tai-Yu Pan, Chenyang Ma, Tianle Chen, Cheng Perng Phoo, Katie Z Luo, Yurong You, Mark Campbell, Kilian Q Weinberger, Bharath Hariharan, and Wei-Lun Chao. Pre-training lidar-based 3d object detectors through colorization. In *ICLR*, 2024.
- Xidong Peng, Xinge Zhu, and Yuexin Ma. Cl3d: Unsupervised domain adaptation for cross-lidar 3d detection. In *AAAI*, 2023.
- Charles R Qi, Hao Su, Kaichun Mo, and Leonidas J Guibas. Pointnet: Deep learning on point sets for 3d classification and segmentation. In *CVPR*, 2017.
- Enver Sangineto, Moin Nabi, Dubravko Culibrk, and Nicu Sebe. Self paced deep learning for weakly supervised object detection. *TPAMI*, 2018.
- Jenny Seidenschwarz, Aljoša Ošep, Francesco Ferroni, Simon Lucey, and Laura Leal-Taixé. Semoli: What moves together belongs together. In *CVPR*, 2024.
- Shaoshuai Shi, Xiaogang Wang, and Hongsheng Li. Pointcnn: 3d object proposal generation and detection from point cloud. In *CVPR*, 2019.
- Shaoshuai Shi, Chaoxu Guo, Li Jiang, Zhe Wang, Jianping Shi, Xiaogang Wang, and Hongsheng Li. Pv-rnn: Point-voxel feature set abstraction for 3d object detection. In *CVPR*, 2020.
- Pei Sun, Henrik Kretzschmar, Xerxes Dotiwalla, Aurelien Chouard, Vijaysai Patnaik, Paul Tsui, James Guo, Yin Zhou, Yuning Chai, Benjamin Caine, et al. Scalability in perception for autonomous driving: Waymo open dataset. In *CVPR*, 2020.
- Darren Tsai, Julie Stephany Berrio, Mao Shan, Eduardo Nebot, and Stewart Worrall. Ms3d: Leveraging multiple detectors for unsupervised domain adaptation in 3d object detection. In *ITSC*, 2023.
- Tsun-Hsuan Wang, Sivabalan Manivasagam, Ming Liang, Bin Yang, Wenyuan Zeng, and Raquel Urtasun. V2vnet: Vehicle-to-vehicle communication for joint perception and prediction. In *ECCV*, 2020a.
- Yan Wang, Wei-Lun Chao, Divyansh Garg, Bharath Hariharan, Mark Campbell, and Kilian Q Weinberger. Pseudo-lidar from visual depth estimation: Bridging the gap in 3d object detection for autonomous driving. In *CVPR*, 2019.
- Yan Wang, Xiangyu Chen, Yurong You, Li Erran Li, Bharath Hariharan, Mark Campbell, Kilian Q Weinberger, and Wei-Lun Chao. Train in germany, test in the usa: Making 3d object detectors generalize. In *CVPR*, 2020b.
- Yan Wang, Junbo Yin, Wei Li, Pascal Frossard, Ruigang Yang, and Jianbing Shen. Ssda3d: Semi-supervised domain adaptation for 3d object detection from point cloud. In *AAAI*, 2023.
- Yi Wei, Zibu Wei, Yongming Rao, Jiaxin Li, Jie Zhou, and Jiwen Lu. Lidar distillation: Bridging the beam-induced domain gap for 3d object detection. In *ECCV*, 2022.
- Qizhe Xie, Minh-Thang Luong, Eduard Hovy, and Quoc V Le. Self-training with noisy student improves imagenet classification. In *CVPR*, 2020a.
- Saining Xie, Jiatao Gu, Demi Guo, Charles R Qi, Leonidas Guibas, and Or Litany. Pointcontrast: Unsupervised pre-training for 3d point cloud understanding. In *ECCV*, 2020b.
- Runsheng Xu, Zhengzhong Tu, Hao Xiang, Wei Shao, Bolei Zhou, and Jiaqi Ma. Cobevt: Cooperative bird’s eye view semantic segmentation with sparse transformers. In *CoRL*, 2022a.
- Runsheng Xu, Hao Xiang, Zhengzhong Tu, Xin Xia, Ming-Hsuan Yang, and Jiaqi Ma. V2x-vit: Vehicle-to-everything cooperative perception with vision transformer. In *ECCV*, 2022b.
- Runsheng Xu, Hao Xiang, Xin Xia, Xu Han, Jinlong Li, and Jiaqi Ma. Opv2v: An open benchmark dataset and fusion pipeline for perception with vehicle-to-vehicle communication. In *ICRA*, 2022c.

- Runsheng Xu, Xin Xia, Jinlong Li, Hanzhao Li, Shuo Zhang, Zhengzhong Tu, Zonglin Meng, Hao Xiang, Xiaoyu Dong, Rui Song, et al. V2v4real: A real-world large-scale dataset for vehicle-to-vehicle cooperative perception. In *CVPR*, 2023.
- Yan Yan, Yuxing Mao, and Bo Li. Second: Sparsely embedded convolutional detection. *Sensors*, 2018.
- Jihan Yang, Shaoshuai Shi, Zhe Wang, Hongsheng Li, and Xiaojuan Qi. St3d: Self-training for unsupervised domain adaptation on 3d object detection. In *CVPR*, 2021.
- Jihan Yang, Shaoshuai Shi, Zhe Wang, Hongsheng Li, and Xiaojuan Qi. St3d++: Denoised self-training for unsupervised domain adaptation on 3d object detection. *TPAMI*, 2022.
- Lei Yang, Kaicheng Yu, Tao Tang, Jun Li, Kun Yuan, Li Wang, Xinyu Zhang, and Peng Chen. Bevheight: A robust framework for vision-based roadside 3d object detection. In *CVPR*, 2023.
- Zetong Yang, Yanan Sun, Shu Liu, Xiaoyong Shen, and Jiaya Jia. Ipod: Intensive point-based object detector for point cloud. *arXiv preprint arXiv:1812.05276*, 2018.
- Junbo Yin, Dingfu Zhou, Liangjun Zhang, Jin Fang, Cheng-Zhong Xu, Jianbing Shen, and Wenguan Wang. Proposalcontrast: Unsupervised pre-training for lidar-based 3d object detection. In *ECCV*, 2022.
- Yurong You, Katie Z Luo, Xiangyu Chen, Junan Chen, Wei-Lun Chao, Wen Sun, Bharath Hariharan, Mark Campbell, and Kilian Q. Weinberger. Hindsight is 20/20: Leveraging past traversals to aid 3d perception. In *ICLR*, 2022a.
- Yurong You, Katie Z Luo, Cheng Perng Phoo, Wei-Lun Chao, Wen Sun, Bharath Hariharan, Mark Campbell, and Kilian Q. Weinberger. Learning to detect mobile objects from lidar scans without labels. In *CVPR*, 2022b.
- Yurong You, Cheng Perng Phoo, Katie Z Luo, Travis Zhang, Wei-Lun Chao, Bharath Hariharan, Mark Campbell, and Kilian Q. Weinberger. Unsupervised adaptation from repeated traversals for autonomous driving. In *NeurIPS*, 2022c.
- Haibao Yu, Yizhen Luo, Mao Shu, Yiyi Huo, Zebang Yang, Yifeng Shi, Zhenglong Guo, Hanyu Li, Xing Hu, Jirui Yuan, et al. Dair-v2x: A large-scale dataset for vehicle-infrastructure cooperative 3d object detection. In *CVPR*, 2022.
- Lunjun Zhang, Anqi Joyce Yang, Yuwen Xiong, Sergio Casas, Bin Yang, Mengye Ren, and Raquel Urtasun. Towards unsupervised object detection from lidar point clouds. In *CVPR*, 2023.
- Hengshuang Zhao, Li Jiang, Jiaya Jia, Philip HS Torr, and Vladlen Koltun. Point transformer. In *ICCV*, 2021.
- Yin Zhou and Oncel Tuzel. Voxelnet: End-to-end learning for point cloud based 3d object detection. In *CVPR*, 2018.
- Ziyue Zhu, Qiang Meng, Xiao Wang, Ke Wang, Liujiang Yan, and Jian Yang. Curricular object manipulation in lidar-based object detection. In *CVPR*, 2023.

Supplementary Material for Learning 3D Perception from Others’ Predictions

In this supplementary material, we provide implementation details and experimental results in addition to the main paper:

- [Sec. S1](#): provides further implementation details.
- [Sec. S2](#): provides additional empirical studies.

S1 ADDITIONAL IMPLEMENTATION DETAILS

The entire training pipeline for the experiments takes 2.5 hours with eight NVIDIA P100 GPUs. During training, we apply conventional data augmentation techniques such as rotation, scaling, and flipping following [Xu et al. \(2023\)](#). For training SECOND ([Yan et al., 2018](#)) in our ablation study, we set the number of epochs to 40, with the remaining training settings the same as PointPillars ([Lang et al., 2019](#)). For the domain adaptation experiments, we decrease the initial learning rate to $2e-4$ and decay it to $2e-6$, and fine-tune the model using the pre-trained parameters.

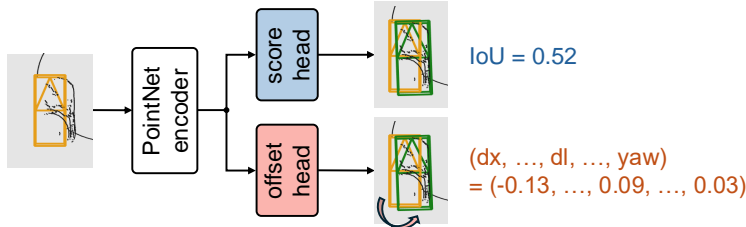


Figure S1: **Ranker architecture.** We give the initial noisy bounding box together with its nearby point clouds to the ranker as inputs and predict the IoU and offset to the ground-truth box.

Ranker training. In the main paper, we train a ranker to select the best candidate from the sampled boxes. Specifically, we build our ranker upon PointNet ([Qi et al., 2017](#)), taking a normalized box and its corresponding points as inputs (see [Fig. S1](#)). We use two linear layers with ReLU non-linearity for both score head and offset head. We crop the point cloud to the range of $\times 3$ of the box size, and predict the IoU and the offset from the object. To prepare the training data, we take the first two frames for each of the 20 clips. We then sample approximately 100 boxes around each ground-truth label, crop out the point cloud around the sampled boxes to serve as training input, and compute the IoU and offset information for labels of the training set. During the ranker training, we also simulate random occlusion and point dropping. For the design of the loss function, we use a weighted combination: $\mathcal{L}_{\text{total}} = 5 * \mathcal{L}_{\text{IoU}} + \mathcal{L}_{\text{offset}}$. Here, the IoU loss \mathcal{L}_{IoU} is defined by the mean squared error between \hat{y} and y , where \hat{y} denotes estimated IoU and y denotes the actual IoU. For the offset prediction loss, since we only use the offset from the top-k boxes, the offset will most likely be applied to high IoU candidate boxes with smaller offset values, as shown in [Fig. S2](#). As such, we are able to prevent training samples with lower IoU and larger offsets from dominating the training process. Based on this observation, we test several different loss functions and see that the ranker performed best using Smooth L1 loss, without adjusting for the sampled box’s offset loss if the IoU is less than 0.3.

Ranker inference. For the ranker refinement module, we sample $N = 512$ boxes in total for both sampling strategies. In the naive sampling strategy, 512 boxes are sampled using Gaussian distributions with translational noise (on xyz) having a standard deviation of 1, and scaling and rotational noise (on lwh, yaw) having a standard deviation of 0.1, all with a mean of zero. For the C2F sampling, we employ both coarse and fine sampling. During coarse sampling, noise is uniformly sampled from $[-1.0, 1.0]$ for xy and from a Gaussian distribution with a standard deviation of 0.5 for z to help us sample $\frac{N}{2} = 256$ boxes. We then select the top $k = 3$ boxes based on the IoU reported

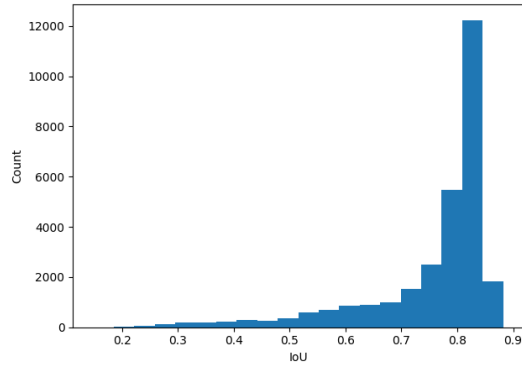


Figure S2: **Top IoU predicted from sampled boxes by ranker.** We computed the statistics for the IoU of the sampled boxes selected by the ranker during refinement. Then, the offset predicted by the ranker was applied to these selected boxes. The result indicates that the offset is most frequently used when the IoU of the box is sufficiently high.

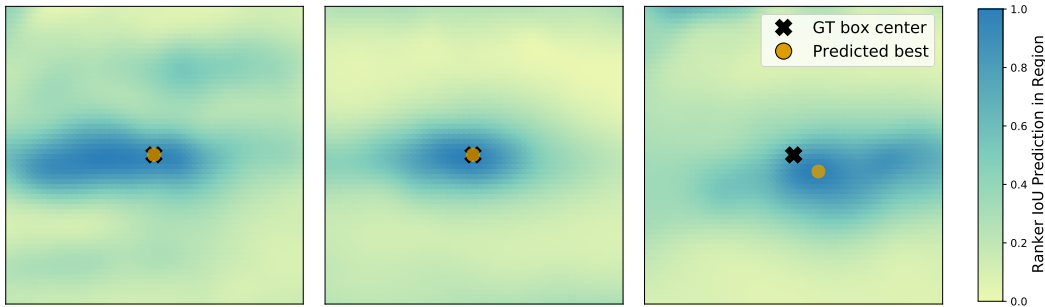


Figure S3: **Ranker IoU prediction behavior.** We visualize the IoU predicted by the ranker on sampled boxes versus the actual ground-truth location. We see that our ranker trained with a handful of annotated frames successfully refines initially mislocalized boxes by giving high scores to samples with more accurate box centers.

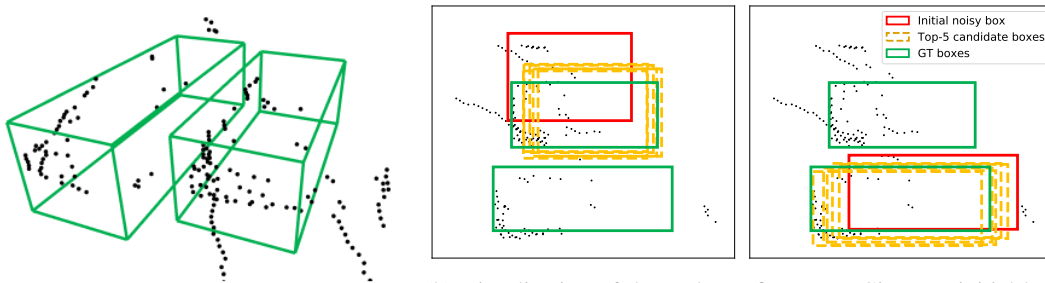
by the ranker, apply the predicted offsets to these boxes, and proceed to sample a total of 256 boxes around each candidate for the fine sampling stage. In this stage, translational noise is sampled from a Gaussian distribution with a standard deviation of 0.25, noise for height and width with a standard deviation of 0.2, length with a standard deviation of 0.4, and rotational noise with a standard deviation of 0.1. We ultimately select the box with the highest IoU among all 256 sampled boxes and apply the predicted offset to obtain the refined label.

S2 ADDITIONAL EMPIRICAL STUDIES

S2.1 ANALYSIS ON SHARING DETECTOR

Table S1: **Detector performance on the ideal case.** R&B-POP also brings meaningful performance gain in the ideal scenario where the object detector can directly be shared.

method	AP @ IoU 0.7			
	0-30m	30-50m	50-80m	0-80m
sharing detector	56.3	29.0	14.9	40.1
+ R&B-POP	60.9	32.3	17.8	44.4



(a) Real example of a scenario where two objects with the **same category** are close.

(b) Visualization of the ranker refinement. Given an initial box assigned to a certain object, our ranker correctly identifies and selects the appropriate objects.

Figure S4: **Additional experiments on a high density of objects.**

Our study introduces a novel learning scenario to build the detector by sharing object box predictions from the reference cars, which is realistic and practical. As shown in [Table 1](#) of the main paper, the pseudo label quality achieved by R&B-POP is as competitive as directly sharing detector, which the scenario faces various constraints (c.f. [Sec. 1](#) and [Sec. 3.1](#)). In this section, to investigate if our method can still improve such cases, we apply our algorithm on top of the object detector shared from the reference car. As shown in [Table S1](#), we observe further performance gain benefit from additional high-quality pseudo labels provided by the reference car in combination with our algorithm. We note that the overall performance is higher than [Table 2](#) in the main paper, as the train and test sets share the same distribution (*i.e.*, clips 1-20 in [Fig. 8](#) in the main paper). This highlights the effectiveness of our study of learning from reference agents' predictions beyond a single agent.

S2.2 ADDITIONAL ANALYSIS ON RANKER

S2.2.1 VISUALIZATION OF PREDICTED SCORES

In the ranker training ablation study in our main manuscript, we mention our ranker design performs well with as little as 40 annotated frames. To illustrate its effectiveness further, we visualize the IoU prediction on sampled boxes *vs.* the actual location of the ground-truth as shown in [Fig. S3](#). We observe that IoUs predicted by our ranker are consistent, and boxes with the highest predicted IoUs are close to the ground-truth. Moreover, the result implies that the ranker can effectively remove the false positives, as the region far away from the actual object tends to be given a lower score.

S2.2.2 RANKER ON HIGH DENSITY OF OBJECTS

To analyze the behavior of our ranker when objects are close, we carefully select examples where cars are close to each other (*i.e.*, within 2.5 meters of the box centers). We note that while the coarse sampling strategy considers translations of one to two meters, compared to the closest centers of two cars (*i.e.*, 2.5 meters), such translations do not necessarily misassign a box to a nearby car. We see that if the reference car predicts a box for each of the two nearby cars, our method can successfully recall both of them. [Fig. S4](#) demonstrates the ranker's performance in correctly identifying and selecting the appropriate vehicles in the coarse sampling stage.

Indeed, the purpose of the ranker is to refine the noisy pseudo labels from the reference to the correct location, size, and pose with respect to the ego agent's view (c.f. [Sec. 3.2](#)). Therefore, even if the reference only predicts a single box or two predicted boxes are refined to the same car, leaving one false negative, our subsequent curriculum self-training is capable of discovering the remaining object.

S2.2.3 EXTENSION TO MULTI-CLASS

In the main paper, we focus on a single category that includes various vehicles (*e.g.*, cars, trucks). Still, the pipeline proposed in the main paper is model-agnostic, meaning it can handle both single-class and multi-class detection. The key is to train separate rankers to capture class-specific information (*e.g.*, sizes, shapes) to provide high-quality pseudo labels for the subsequent distance-based curriculum self-training.

Table S2: Extension of ranker to multi-class refinement.

pseudo label	car	truck
	rec. / prec.	rec. / prec.
initial boxes	56.1 / 71.0	57.2 / 61.0
+ our refinement	60.6 / 76.7	64.2 / 68.4



(a) Real example of a scenario where two objects with **different categories** ('car' and 'truck') are close. (b) Visualization of two class-specific rankers (*i.e.*, car ranker and truck ranker). Each ranker assigns different scores to different bounding boxes but predicts the highest score for the desired class.

Figure S5: Additional experiments on multi-class for ranker.

Therefore, we explore the multi-class setup by further separating regular cars and trucks in V2V4Real (Xu et al., 2023) and employing car-specific and truck-specific rankers, respectively. As shown in Table S2, we observe significant improvements in label quality for both classes. Additionally, we conduct a study with selecting cases where nearby objects belong to different categories (*i.e.*, car vs. truck). This is considered challenging because cars and trucks have similar shapes but differ mainly in size. As shown in Fig. S5, we see that the two rankers capture class-specific information and score boxes of different sizes differently, for example, the car ranker gives smaller-size boxes a higher score. We believe such a property would reduce the chance of mistakenly assigning a box of one class to a nearby object of a different class. Moreover, by experimenting with tens of such cases with nearby objects of different classes, we find that the class-specific rankers can correctly maintain class distinctions (*i.e.*, not flipping the classes) with 72.5%, indicating that the rankers effectively capture class-specific information to provide high-quality pseudo labels.

S2.3 ADDITIONAL ANALYSIS ON SELF-TRAINING

S2.3.1 COMBINING DIFFERENT SETS OF PSEUDO LABELS

Table S3: Analysis on pseudo label combination during self-training. [†] distance-based curation: using only R 's predictions within its 40m.

using R 's pred	distance-based curation [†]	AP @ IoU 0.5			
		0-30m	30-50m	50-80m	0-80m
x (main paper)	-	73.3	43.3	23.3	56.5
o	x	71.8	41.5	26.5	55.1
o	o	74.5	42.0	25.1	57.0

In the main paper, we propose to utilize the predicted output of the trained detector, rather than the initially provided predictions from the reference car. In this section, we investigate different combining strategies. First, we naively combined the ego's and reference's predictions in stage 2.

Table S4: **Additional experimental results on OPV2V dataset (Xu et al., 2022c)**. The performance is reported on PointPillars (Lang et al., 2019) with 64-beam LiDAR. The evaluation metric is AP at IoU 0.5. : uses GT labels.

	pseudo label	box refinement	self-training	time delay = 1				time delay = 2			
				0-30m	30-50m	50-80m	0-80m	0-30m	30-50m	50-80m	0-80m
①	<i>R</i> 's pred	-	-	84.4	62.7	31.1	71.7	80.9	58.6	22.0	67.3
②	<i>R</i> 's GT	-	-	86.7	65.7	33.6	74.2	84.7	65.1	27.8	72.0
③	<i>R</i> 's pred	ranker	-	92.3	68.4	26.1	77.0	91.1	62.2	18.6	73.5
④	<i>R</i> 's pred	-	distance-based curriculum	94.4	74.7	28.2	80.8	94.1	72.8	28.0	79.9
⑤	<i>R</i> 's pred	ranker	distance-based curriculum	96.1	77.4	34.6	83.2	95.3	74.3	31.9	81.4
♣	<i>E</i> 's GT	-	-	97.6	89.4	68.4	90.8	97.6	89.4	68.4	90.8

As shown in Table S3, the overall performance (0-80m) dropped from 56.5 (row 1) to 55.1 (row 2). However, we also observe that the performance in the 50-80m range increased from 23.3 to 26.5. We hypothesize that predictions closer to the ego agent are actually farther from the reference, introducing noisier pseudo labels for the ego agent with the naive solution. Conversely, the reference provides more confident predictions for objects closer to it, which are farther from the ego-agent. Based on this assumption, we further explore a simple distance-based curation strategy, combining only predictions within 40m of the reference. As shown in the table, this approach improves the overall performance (0-80m) from 56.5 (row 1) to 57.0 (row 3) and maintained the performance in the 0-30m range (73.3 vs 74.5). These simple experiments demonstrate the potential for many interesting ideas that can be built upon our proposed learning scenario, and we leave it for the future study.

S2.4 ADDITIONAL RESULTS ON OTHER DATASET

In the main paper, we conduct experiments on the real-world dataset, V2V4Real (Xu et al., 2023). To see the generalizability of R&B-POP, we also evaluate our method on OPV2V (Xu et al., 2022c), a simulation dataset containing 2~7 connected cars within the scene. To suit our study, we re-split the entire 69 clips into 33 and 36 similar to Fig. 8 in the main paper. Also, we only use frames where the distance between the ego car and the reference car is within 90m. To simulate real-world noise, we sample random Gaussian noise with a zero mean and 0.2 standard deviation for localization error and consider a time delay of one and two frames. We set the training epoch to 15, and other hyperparameters remain the same. We use a total of 72 frames for the ranker training, which is two frames per ego car training clip. As shown in Table S4, we see that R&B-POP consistently improves performance on different data and settings, witnessing the general applicability of our method.

S2.4.1 MULTIPLE REFERENCE CARS

Table S5: **Experiments on the number of reference cars**. Detection performance improves further as the ego car gathers more initial pseudo-labels from multiple reference cars. The evaluation metric is AP at IoU 0.5.

# reference car	time delay = 1				time delay = 2			
	0-30m	30-50m	50-80m	0-80m	0-30m	30-50m	50-80m	0-80m
1	96.1	77.4	34.6	83.2	95.3	74.3	31.9	81.4
2	94.3	78.2	43.5	83.4	96.1	79.1	38.6	84.0

Since OPV2V (Xu et al., 2022c) has scenes with more than one reference car, we investigate the relationship between the number of reference cars and detection performance. We use non-maximum suppression with a ranker score to combine two sets of pseudo labels. As shown in Table S5, we see that leveraging the predicted boxes from more reference cars improves final detection performance as different sets of pseudo labels from different views can supplement each other.

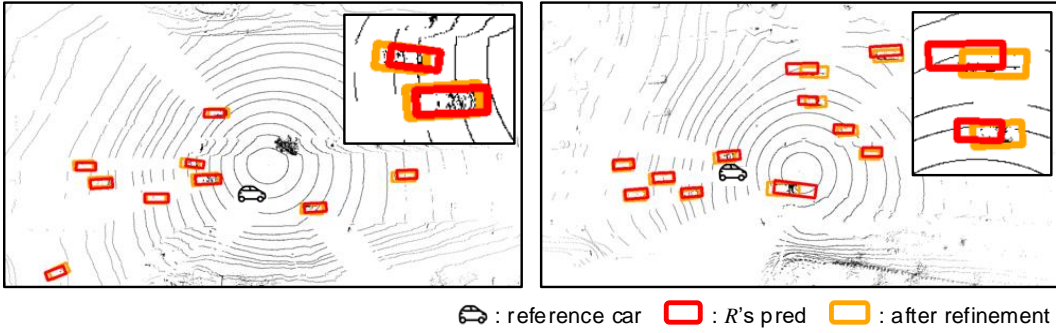


Figure S6: Additional qualitative results of our ranker.

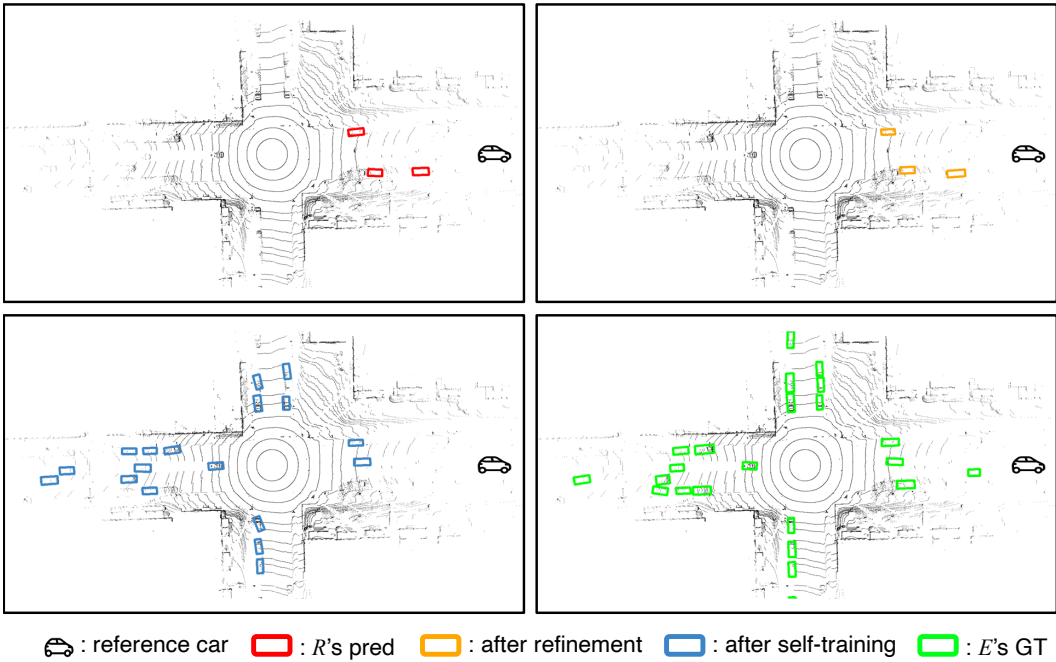


Figure S7: Additional qualitative results of our overall pipeline.

S2.5 ADDITIONAL QUALITATIVE RESULTS

We provide additional visual results on V2V4Real (Xu et al., 2023) in Fig. S6 and Fig. S7. Notably, our pipeline improves pseudo label quality by adjusting mislocalization and by discovering and filtering out boxes appropriately.